A Survey of Robot Interaction Control Schemes with Experimental Comparison

Stefano Chiaverini, Bruno Siciliano, *Senior Member, IEEE*, and Luigi Villani, *Member, IEEE*

Abstract—A great many control schemes for a robot manipulator interacting with the environment have been developed in the literature in the past two decades. This paper is aimed at presenting a survey of robot interaction control schemes for a manipulator, the end effector of which comes in contact with a compliant surface. A salient feature of the work is the implementation of the schemes on an industrial robot with open control architecture equipped with a wrist force sensor. Two classes of control strategies are considered, namely, those based on static model-based compensation and those based on dynamic model-based compensation. The former provide a good steady-state behavior, while the latter enhance the behavior during the transient. The performance of the various schemes is compared in the light of disturbance rejection, and a thorough analysis is developed by means of a number of case studies.

Index Terms—Force control, force sensor, impedance control, robots, stiffness control.

I. INTRODUCTION

CONTROLLING the interaction of a robot manipulator with the environment is crucial for accomplishing a variety of tasks in industrial applications, such as mechanical part mating, object contour surface tracking, and employment of tools for machining mechanical parts [1].

When in contact, the end-effector position is constrained along certain task-space directions by the presence of the environment, and a suitable compliant behavior of the manipulator is required to accommodate the interaction. The basic strategy to achieve this purpose is stiffness control [2] which corresponds to proportional-derivative (PD) control with gravity compensation. The amount of the proportional gain sets the manipulator (active) stiffness which has to be properly tuned versus the surface (passive) stiffness.

Stiffness control is designed to achieve a desired static behavior of the interaction. In order to achieve a desired dynamic behavior, the actual mass and damping at the contact are to be considered besides the stiffness, leading to impedance control [3]. The resulting impedance is a function of the

manipulator configuration; measurement of contact force is needed to obtain a configuration-independent impedance.

A common shortcoming of the above strategies is that the contact force is controlled only indirectly by acting on the impedance parameters. An effective way to realize direct force control [4] is to close an outer force feedback loop around an inner velocity or position feedback loop [5], where an integral action on the force error is typically needed to regulate the contact force to a desired value [6].

In order to provide motion control capabilities, the parallel force/position control approach can be adopted [7], where a position feedback loop acts in parallel to a force feedback loop. Dominance of the force control action ensures force regulation along the constrained task-space directions, while the position control action can be designed to achieve either regulation or tracking of the end-effector position along the unconstrained task-space directions.

All of the above strategies are conceived to handle interaction without knowledge of a geometric description of the contact. It should be clear, however, that it is advantageous to exploit such information whenever available, so as to discriminate between task components to be force controlled and task components to be position controlled [8], leading to the well-known hybrid position/force control [9] and subsequent developments [10], [11].

The aim of this paper is to present a survey of several interaction control schemes that are developed according to the strategies of stiffness control, impedance control, force control, and parallel force/position control. Hybrid position/force control is not considered, since scarce information about the contact surface is assumed.

In order to provide a unifying perspective, the above strategies are framed into two classes, namely, those using static model-based compensation, and those using dynamic model-based compensation. The former class is aimed at guaranteeing good system performance at steady state and, thus, the only requirement is the knowledge of manipulator kinematics and gravity torques; impedance control with static model-based compensation (hereafter called stiffness control), force control, and parallel force/position regulator are considered. On the other hand, the latter class is aimed at enhancing the behavior of the system during the transient and, thus, it is required to know the full dynamic model and have a force sensor; impedance control with dynamic model-based compensation (hereafter called impedance control), impedance control with inner position loop, force control with inner

velocity loop, force control with inner position loop, and parallel force/position control are considered.

The results of the implementation of the various interaction control schemes on an industrial robot equipped with a commercially available wrist force sensor are presented. A salient feature of the present work is the use of the open operational mode of the robot control architecture which allows execution of control algorithms on a standard PC, the ISA bus of which is interfaced to the VME bus of the industrial control unit [12]. Such open control architecture is available on the market, reflecting a current trend in industrial robot manufacturers [13], e.g., ABB, Comau, Kuka, and Mitsubishi.

The performance of the schemes and, in particular, their capabilities of disturbance rejection are analyzed in a number of experimental case studies throughout the paper. In order to allow for a fair comparison of the schemes, the gains of the various control actions were tuned via extensive MATLAB simulations prior to the experiments (simulation results are omitted here for brevity), so as to ensure a comparable behavior in terms of system bandwidth and steady-state precision, whenever possible.

It is believed that the present survey with experimental validation might provide useful guidelines for implementation of interaction control schemes on an industrial robot with open control architecture. Nevertheless, it is understood that more insight about how the performance of the various schemes is affected by the choice of different control gains should be acquired by referring to the proper literature, which is cited for each class of schemes throughout the paper.

II. EXPERIMENTAL SETUP

The setup available in the PRISMA Lab consists of an industrial robot, Comau SMART-3 S. The robot manipulator has a six-revolute-joint anthropomorphic geometry with nonnull shoulder and elbow offsets and nonspherical wrist. The joints are actuated by brushless motors via gear trains; shaft absolute resolvers provide motor position measurements. The robot is controlled by an open version of the C3G 9000 control unit which has a VME-based architecture with two processing boards (Robot CPU and Servo CPU) both based on a Motorola 68020/68882, where the latter has an additional digital signal processor (DSP) and is in charge of trajectory generation, inverse kinematics, and joint position servo control. Connection of the VME bus to the ISA bus of a standard PC is made possible by two Bit 3 Computer bus adapter boards, and the PC and C3G controller communicate via the shared memory available in the Robot CPU [12]; a PC Pentium/133 is used. Time synchronization is implemented by interrupt signals from the C3G to the PC with data exchange every 1 ms. A set of C routines is available to drive the bus adapter boards.

The open version of the control unit allows seven different operational modes, including the standard mode available on the industrial version of the controller. To implement force/position control schemes, the operational mode number 4 has been used, in which the PC is in charge of computing the control algorithm and passing the references to the current servos through the communication link at 1-ms sampling
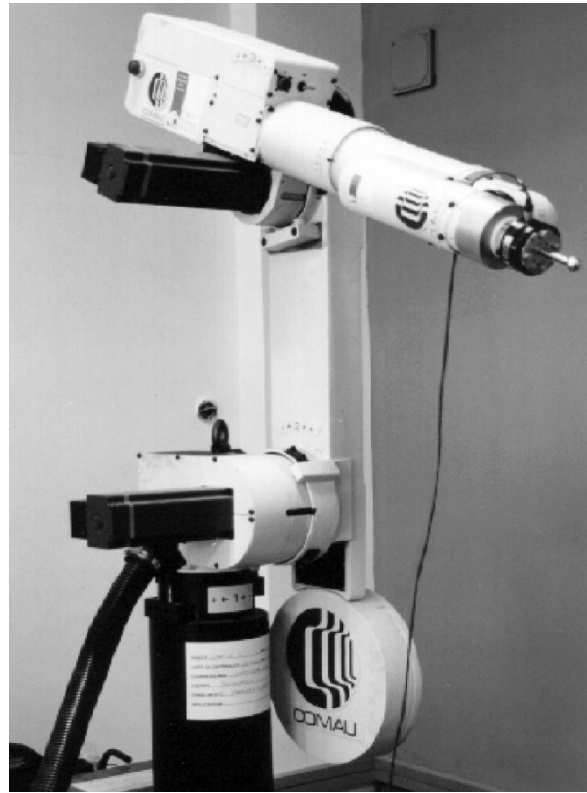

Fig. 1. Industrial robot Comau SMART-3 S with force/torque sensor ATI FT30-100 and built end effector available in the PRISMA Lab.

time. Joint velocities are reconstructed through numerical differentiation of joint position readings.

A six-axis force/torque sensor ATI FT30-100 with force range of ± 130 N and torque range of ± 10 N·m is mounted at the manipulator's wrist. The sensor is connected to the PC by a parallel interface board which provides readings of six components of generalized force at 1 ms. An end effector has been built as a stick with a sphere at the tip, both made of steel.

A picture illustrating the robot with the wrist force sensor and the built end effector is given in Fig. 1, while a schematic of the open control architecture is depicted in Fig. 2.

For the purpose of this work, only the inner three joints are considered and the outer three joints are mechanically braked. Three-degree-of-freedom tasks are considered, involving end-effector position and linear force. The environment is constituted by a cardboard box, where the stiffness depends on the contact point and is about 10^4 N/m. This choice is motivated by the desire of safely analyzing the performance of each control scheme where the interaction with the environment encompasses an unplanned transition from noncontact to contact at nonnegligible end-effector speed. On the other hand, for larger values of contact stiffness, a more accurate planning of constrained and unconstrained motion would be needed, and contact transition at very low speed should be ensured.

III. MODELING

The dynamic model of the three-joint rigid robot manipulator can be written in the form

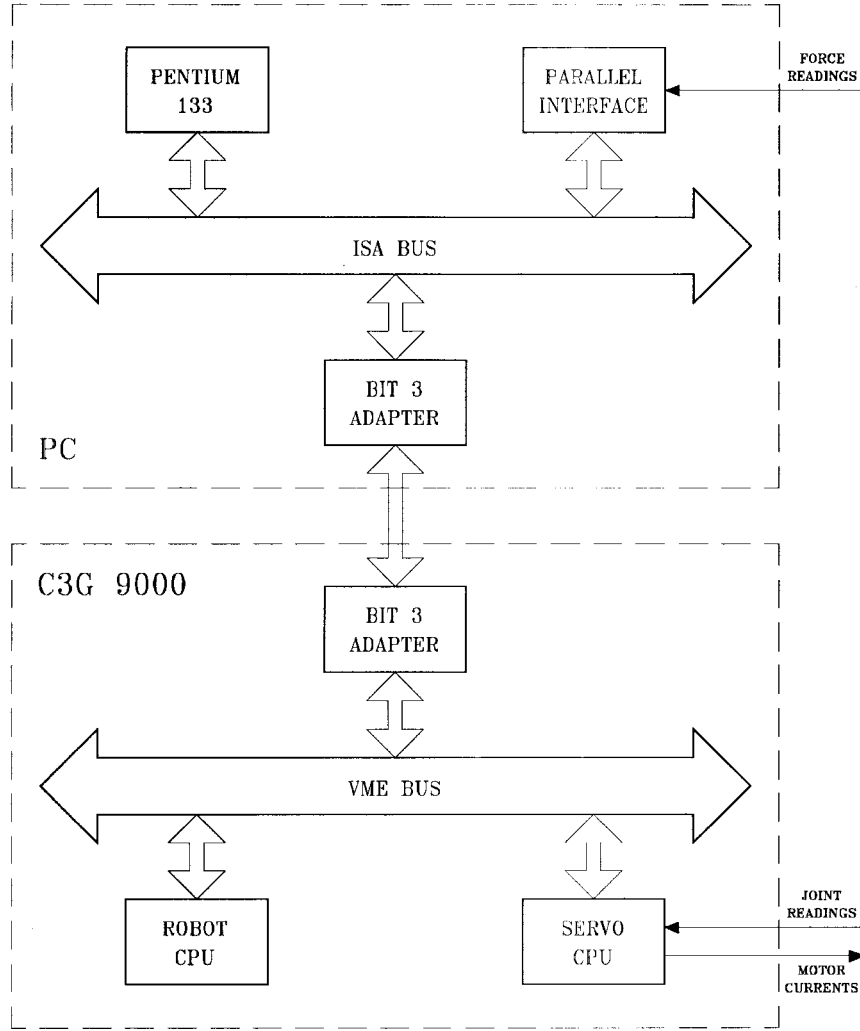$$B(q)\ddot{q} + C(q,\dot{q})\dot{q} + d(q,\dot{q}) + g(q) = u - J^{\mathrm{T}}(q)f \quad (1)$$

Fig. 2. Schematic of open control architecture.

where q is the (3×1) vector of joint variables, B is the (3×3) symmetric inertia matrix, $C\dot{q}$ is the (3×1) vector of Coriolis and centrifugal torques, d is the (3×1) vector of friction torques, g is the (3×1) vector of gravitational torques, u is the (3×1) vector of driving torques, f is the (3×1) vector of contact forces exerted by the end effector on the environment, and J is the (3×3) Jacobian matrix relating joint velocities $\dot{q}$ to the (3×1) vector of end-effector velocities $\dot{p}$, i.e.,

$$\dot{p} = J(q)\dot{q} \qquad (2)$$

which is assumed to be nonsingular.

For analysis purposes, the environment is simply modeled as a frictionless and elastically compliant plane. A point contact is considered and the contact force is expressed as

$$f = K(p - p_0) \qquad (3)$$

where p is the end-effector position at the contact point, p_0 is a point of the plane at rest, and

$$K = k\,nn^T \qquad (4)$$

is the (3×3) constant symmetric stiffness matrix, n being the unit vector of the direction normal to the contact plane, and $k > 0$ the stiffness coefficient; note that all quantities are expressed in the common reference frame, and the model (3) holds only when the end effector is in contact with the environment.

IV. INTERACTION CONTROL SCHEMES WITH STATIC MODEL-BASED COMPENSATION

This class of schemes is aimed at guaranteeing good system performance at steady state. Hence, the only model-based compensation requirements concern static terms, i.e., the manipulator Jacobian and the gravity torques.

A. Stiffness Control

Stiffness control [2] derives from a position control scheme of PD type with gravity compensation. Let p_d denote the desired end-effector position; the driving torques are chosen as

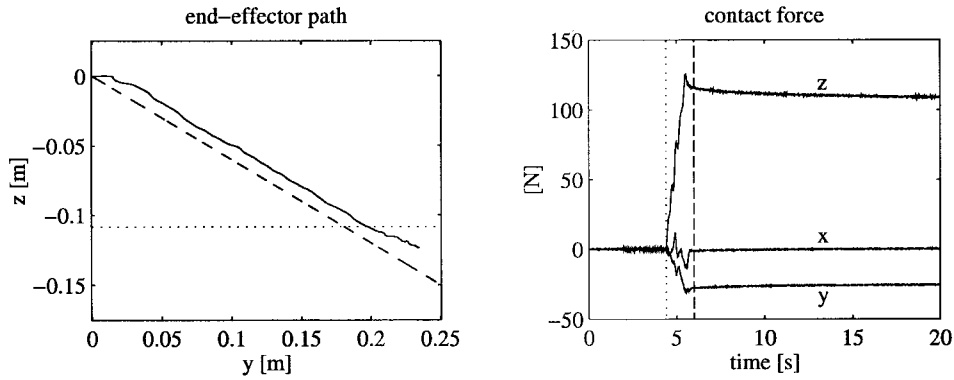$$u = J^T(q)k_p(p_d - p) - k_v\dot{q} + g(q) \qquad (5)$$

Fig. 3.   Experimental results under stiffness control.

where k_p is the gain of an active stiffness on the end-effector position error, and k_v is the gain of a joint damping action. The purpose of this control is to make the end effector compliant with respect to contact forces by acting on k_p. For such a reason, this strategy is also referred to in the literature as (active) compliance control; also, since damping is controlled besides stiffness, the control law (5) can be regarded as an impedance control [3] with static model-based compensation. Notice that no force measurement is required.

The above control law provides a locally isotropic stiffness along the task-space directions; however, the static behavior can be made anisotropic by choosing a suitable positive definite matrix gain in lieu of a scalar gain in (5). Scalar gains will be adopted hereafter in all the control schemes.

Substituting the control law (5) in (1) and accounting for (3) and (4) gives at steady state the following end-effector position and contact force:

$$p_\infty = nn^T \left(\frac{k_p}{k+k_p} \left(p_d - \frac{1}{k_p} \, \delta_\infty \right) + \frac{k}{k+k_p} \, p_0 \right)$$
$$+ (I - nn^T) \left(p_d - \frac{1}{k_p} \, \delta_\infty \right) \qquad (6)$$

$$f_\infty = \frac{kk_p}{k+k_p} \, nn^T \left(p_d - \frac{1}{k_p} \, \delta_\infty - p_0 \right) \qquad (7)$$

where the components along the constrained (nn^T) and unconstrained $(I - nn^T)$ task-space directions have been separated, and δ_∞ is the steady-state value of the term

$$\delta = J^{-T} d. \qquad (8)$$

Stability analysis of the closed-loop system (1) under control (5) derives from the seminal work in [14] using energy-based Lyapunov functions and is discussed in, e.g., [15].

Notice that the friction torques may, in general, be nonnull at steady state (e.g., Coulomb friction), in which case they provoke a bias $(-1/k_p)\delta_\infty$ on the desired end-effector position. Likewise, a mismatching on gravity compensation $\hat{g}$ would generate an additional term in (8), i.e., $\delta = J^{-T}(d + g - \hat{g})$.

Unless for the above bias, from (6) it can be recognized that the desired end-effector position is reached along the unconstrained task-space directions, while an error occurs along the constrained task-space direction depending on p_0,

as well as on the amount of active stiffness (k_p) versus environment stiffness (k). From (7), the contact force along the constrained task-space direction is determined accordingly, in that if $k_p \gg k$ the equivalent stiffness is mostly due to the environment, while if $k_p \ll k$ the equivalent stiffness is mostly due to the manipulator.

In order to show the performance of stiffness control, a case study was developed on the experimental setup described in Section II.

The task consisted of a straight line motion in the yz plane with an end-effector (horizontal) displacement of 0.25 m along y and (vertical) displacement of -0.15 m along z. The trajectory along the path was generated according to a trapezoidal velocity profile with cubic blends, and null initial and final velocities and accelerations, and a duration of 6 s. The surface of the cardboard box is nearly flat and was placed (horizontally) in the xy plane in such a way as to obstruct the desired end-effector motion. The gains of the control action in (5) were set to $k_p = 8000$ N/m and $k_v = 200$ N·m·s/rad; note that k_p was chosen on the basis of a tradeoff between position accuracy during the unconstrained motion and compliant behavior at the end effector (limited values of contact force) during the constrained motion, while k_v was chosen so as to guarantee a well-damped behavior.

The results are presented in Fig. 3 in terms of the desired (dashed) and the actual (solid) end-effector path, together with the time history of the contact force; in order to facilitate interpretation of the results, the approximate location (dotted) of the surface is illustrated on the plot of the end-effector path, while the instant of contact (dotted line) and the instant of the end of the motion trajectory (dashed line) are evidenced on the plot of the contact force.

It can be recognized that path tracking accuracy is rather poor during execution of the whole task. On the other hand, the contact force along z reaches a steady-state value, but its amount is rather large. Reduction of the contact force could be obtained by decreasing k_p, although at the expense of a larger end-effector position error. If a force sensor were available, k_p could be conveniently adjusted before and after the contact as a function of the measured force.

Finally, notice the presence of an appreciable value of contact force along y at steady state due to contact friction, which was not modeled in the above analysis.
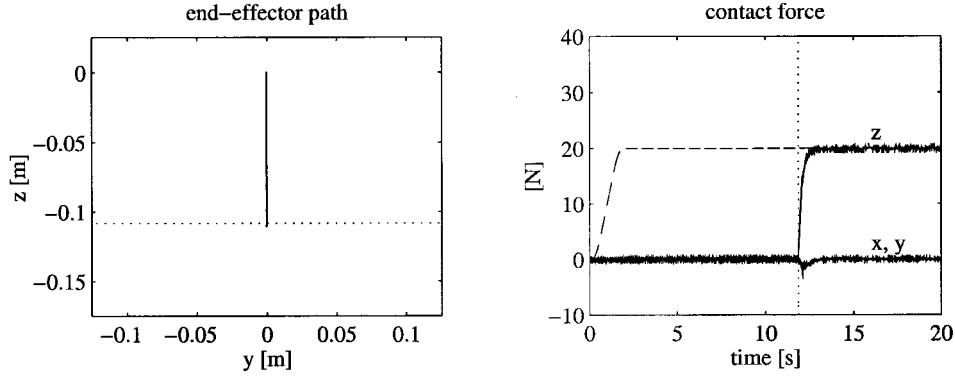
Fig. 4. Experimental results under force control.

B. Force Control

If force measurement is available, it is possible to regulate the contact force to a desired value. Force control [4] can be entrusted to the adoption of a proportional-integral (PI) action on the force error plus desired force feedforward. Let f_d denote the constant desired contact force which shall be aligned with n [in a consistent way with the model (3) and (4)]; the driving torques are chosen as

$$u = J^T(q)(k_P(p_f - p) + f_d) - k_v \dot{q} + g(q) \qquad (9)$$

with

$$p_f = k_c(f_d - f) + k_{ic} \int_0^t (f_d - f) \, d\tau \qquad (10)$$

where k_c is the gain of a proportional action on the force error, and k_{ic} is the gain of an integral action on the force error. Notice in (9) that an inner loop on the end-effector position is used, which, in turn, corresponds to leaving the proportional action for motion control in the task space; this is in accordance with the fact that a position feedback loop is usually available in an industrial robot controller.

Substituting the control law (9) and (10) in (1) and accounting for (3) and (4) gives at steady state the contact force

$$f_\infty = f_d. \qquad (11)$$

Thanks to the use of the integral action, the term in (8) has no effect at steady state. Notice, however, that end-effector position is not controlled at all. Stability of the closed-loop system (1) under control (9) is discussed in, e.g., [15], and robustness issues are considered in [16].

In order to show the performance of force control, a case study was developed on the experimental setup described in Section II.

The end effector was placed in the same initial position as for the previous case study, but, of course, no trajectory could be assigned to the end-effector position. The desired force along z was taken to 20 N according to a trapezoidal velocity profile with cubic blends, and null initial and final first and second time derivatives, and a duration of 2 s. The constant value was kept for the remaining portion of the task. The gains of the control action in (9) and (10) were set to $k_p = 300\,000$

N/m, $k_v = 3000$ N·m·s/rad, $k_c = 0$, and $k_{ic} = 0.0005$ m/(N·s); note that the proportional action on the force error does not vanish because of the null k_c, since the force feedforward in (9) combined with the contact force term in (1) is, in turn, equivalent to a unitary proportional action.

The results are presented in Fig. 4 in terms of the end-effector path, together with the time history of the desired (dashed) and the actual (solid) contact force. As above, the approximate location (dotted) of the surface is illustrated on the plot of the end-effector path, while the instant of contact (dotted line) is evidenced on the plot of the contact force.

Initially, the desired force trajectory causes a downward vertical motion, since the end effector is required to push in the air; this brings the end effector to come in contact with the surface at $t = 12$ s. Then, the contact force is successfully regulated to the desired value. The components of contact friction force along x and y are nearly zero, since no motion is commanded along those directions.

C. Parallel Force/Position Regulator

In order to combine the features of stiffness control and force control, a parallel force/position regulator can be designed, where a PI force control action plus desired force feedforward is used in parallel to a PD position control action. The driving torques are chosen as

$$u = J^T(q)\left(k_P(p_d - p) + f_d + k_f(f_d - f) \right.$$

$$\left. + k_i \int_0^t (f_d - f) \, d\tau \right) - k_v \dot{q} + g(q) \quad (12)$$

where the integral action on the force error ensures dominance of the force loop over the position loop.

Substituting the control law (12) in (1) and accounting for (3) and (4) gives at steady state the following end-effector position and contact force:

$$p_\infty = nn^T\left(\frac{1}{k} f_d + p_0 \right) + (I - nn^T)\left(p_d - \frac{1}{k_p} \delta_\infty \right) \quad (13)$$

$$f_\infty = f_d \qquad (14)$$
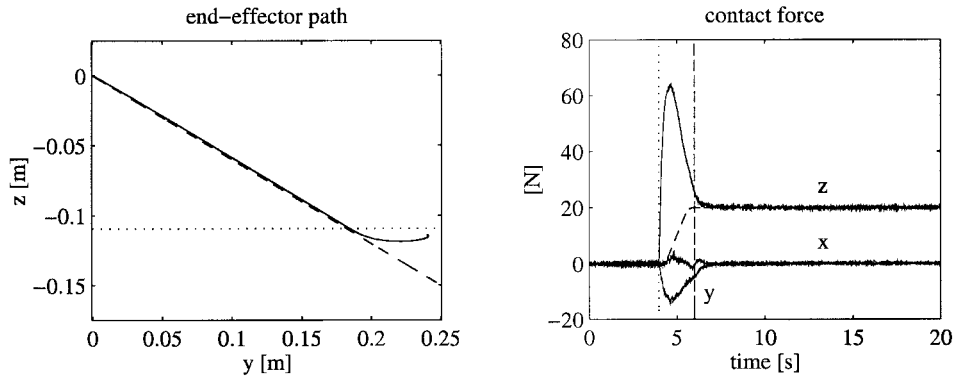
with δ as in (8).

Fig. 5.   Experimental results under parallel force/position regulator.

Equation (14) yields contact force regulation along the constrained task space direction [as in (11)], while (13) yields end-effector position regulation along the unconstrained task-space directions unless for the bias $(-1/k_P)\delta_\infty$ [as in (6)]. Stability of the closed-loop system (1) under control (12) using energy-based Lyapunov functions is discussed in [17].

In order to show the performance of parallel force/position regulator, a case study was developed on the experimental setup described in Section II.

The end effector was placed in the same initial position as for the previous case studies. The end-effector task was the same as for the case study described in Section IV-A, while the same force trajectory as in Section IV-B was imposed as soon as contact is detected. The gains of the control action in (12) were set to $k_p = 300\,000$ N/m, $k_v = 3000$ N·m·s/rad, $k_f = 0$, and $k_i = 150$ m/(N·s); the same argument as in the previous case study holds with respect to the proportional action on the force error.

The results are presented in Fig. 5 in terms of the desired (dashed) and the actual (solid) end-effector path, together with the time history of the desired (dashed) and the actual (solid) contact force. As above, the approximate location (dotted) of the surface is illustrated on the plot of the end-effector path, while the instant of contact (dotted line) and the instant of the end of the motion trajectory (dashed line) are evidenced on the plot of the contact force.

It can be recognized that path tracking accuracy is satisfactory during unconstrained motion, even with a simple PD position control action plus gravity compensation. On the other hand, during constrained motion, after a transient the contact force reaches the desired value; the peak on the component along z is due to the nonnull value of end-effector velocity at the contact, as well as to the imposed motion into the surface, whereas the appreciable deviation from zero of the component along y can be imputed to contact friction and local deformation of the surface resulting from the imposed end-effector motion.

In any case, both components of contact friction force along x and y are regulated to zero in view of the integral action on all the components of the force error, whereas the component along z reaches a steady-state value which guarantees exact force regulation according to (13) and (14).

V. INTERACTION CONTROL SCHEMES WITH DYNAMIC MODEL-BASED COMPENSATION

In order to enhance the dynamic behavior of the system, full compensation of the terms in the dynamic model, as well as force measurement, are needed.

According to the well-known concept of inverse dynamics [18], the driving torques are chosen as

$$u = B(q)J^{-1}(q)(a - \dot{J}(q,\dot{q})\dot{q}) + C(q,\dot{q})\dot{q}$$
$$+ \hat{d}(q,\dot{q}) + g(q) + J^T(q)f \quad (15)$$

where $\hat{d}$ denotes the available estimate of the friction torques and f is the measured contact force.

In the case of a kinematically redundant manipulator (nonsquare Jacobian matrix), a dynamically consistent generalized inverse of the Jacobian can be adopted and the redundant degrees of freedom can be exploited to meet additional constraints besides the end-effector task [19].

Notice that it is reasonable to assume accurate compensation of the terms in the dynamic model (1), e.g., as obtained by a parameter identification technique [20] except for the friction torques. To the scope of the present work, the following model of friction has been used in the implementation of (15):

$$\hat{d} = D\dot{q} \quad (16)$$

which corresponds to including joint viscous friction only [21].

Substituting the control law (15) in (1) and accounting for the time derivative of (2) gives

$$\ddot{p} = a - \eta \quad (17)$$

that is a resolved end-effector acceleration for which the term

$$\eta = JB^{-1}\left(d - \hat{d}\right) \quad (18)$$

can be regarded as a disturbance. In the case of mismatching on other terms in the dynamic model (1), such a disturbance would include additional contributions. The new control input a is available to provide interaction control capabilities.

A drawback of inverse dynamics control is that tracking control performance relies on the feedback linearization of the system. This argument has motivated research of alternative model-based control schemes which do not compensate for
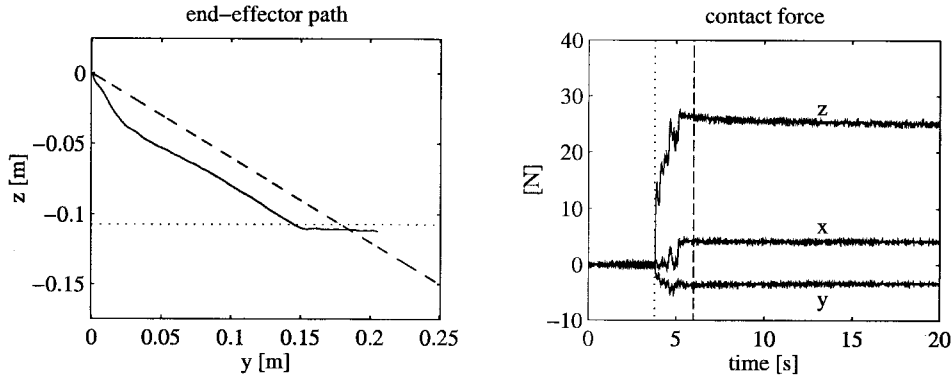
Fig. 6. Experimental results under impedance control.

system dynamics and, thus, are expected to exhibit better robustness to model uncertainties, e.g., Lyapunov-based controllers and passivity-based controllers. In case of unmodeled dynamics or parameter uncertainties, the above control schemes can be made robust or adaptive, respectively. Such schemes are outside the scope of the present work; see [22] for further discussion of model-based control, stability, and robustness. Examples of model-based interaction controllers not using inverse dynamics can be found in, e.g., [23]–[28].

A. Impedance Control

Impedance control [3] is aimed at realizing a desired dynamic relationship between end-effector position and contact force. This behavior was already achieved by the stiffness control in Section IV-A, but, thanks to the use of a dynamic model-based compensation, now the impedance behavior can be assigned independently of the manipulator dynamics. The new control input in (17) is chosen as

$$a = \ddot{p}_d + \frac{d_d}{m_d}\left(\dot{p}_d - \dot{p}\right) + \frac{k_d}{m_d}\left(p_d - p\right) - \frac{1}{m_d}f \quad (19)$$

where the parameters m_d, d_d, and k_d are, respectively, the mass, damping, and stiffness of the desired mechanical impedance between the end-effector position error and the contact force, unless for the disturbance. The closed-loop system dynamic behavior is described by

$$m_d(\ddot{p}_d - \ddot{p}) + d_d(\dot{p}_d - \dot{p}) + k_d(p_d - p) = f + m_d\eta. \quad (20)$$

Notice that feedforward desired acceleration and velocity terms are usually not present in the impedance equation, so as to guarantee passivity of the system when the end effector is in contact with the environment [29]. Notwithstanding, such terms are introduced to the purpose of ensuring full end-effector trajectory tracking before contact and tracking along the unconstrained task-space directions after contact. Also, robustness of impedance control to the amount of contact stiffness was discussed in [30] and [31].

On the other hand, the behavior of the system at steady state is substantially equivalent to that with stiffness control in (6) and (7), where k_d in (19) plays the role of k_p in (5). In fact, substituting the control law (15) and (19) in (1) and

accounting for (3) and (4) gives at steady state the following end-effector position and contact force:

$$p_\infty = nn^T\left(\frac{k_d}{k + k_d}\left(p_d - \frac{m_d}{k_d}\eta_\infty\right) + \frac{k}{k + k_d}p_0\right) + \left(I - nn^T\right)\left(p_d - \frac{m_d}{k_d}\eta_\infty\right) \quad (21)$$

$$f_\infty = \frac{kk_d}{k + k_d}nn^T\left(p_d - \frac{m_d}{k_d}\eta_\infty - p_0\right) \quad (22)$$

where η_∞ is the steady-state value of η in (18).

In order to show the performance of impedance control, a case study was developed on the experimental setup described in Section II.

The end effector was placed in the same initial position as for the previous case studies, and the same trajectory as for the case study described in Section IV-A was assigned. The impedance parameters in (19) were set to $m_d = 10$ kg, $d_d = 255$ N·s/m, and $k_d = 500$ N/m, where the choice of k_d was aimed at obtaining a value of the contact force along z of approximately 20 N with the available estimate of the surface stiffness.

The results are presented in Fig. 6 in terms of the desired (dashed) and the actual (solid) end-effector path, together with the time history of the contact force. As above, the approximate location (dotted) of the surface is illustrated on the plot of the end-effector path, while the instant of contact (dotted line) and the instant of the end of the motion trajectory (dashed line) are evidenced on the plot of the contact force.

It can be recognized that path tracking accuracy is poor during execution of the whole task; this is imputable to the disturbance term on the right-hand side of (20). On the other hand, the contact force along z is limited during the transient and reaches a constant value at steady state. Improvement of the position tracking accuracy might be achieved by increasing k_d, however, this would give rise to larger contact forces. Finally, notice the presence of an appreciable value of contact friction force along both x and y at steady state, which is caused by the end-effector position deviation along both x and y (although the former is not visible in the figure).

In order to improve path tracking accuracy, an approximate compensation of static friction at the joints can be added to
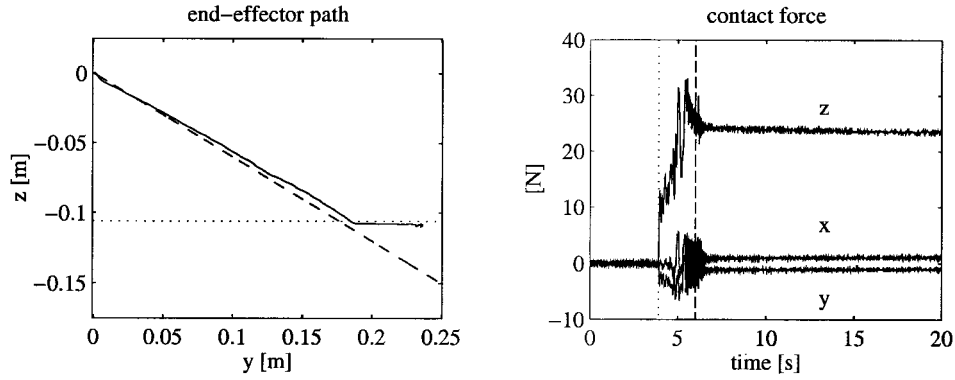
Fig. 7. Experimental results under impedance control with Coulomb friction compensation.

(16), e.g., as

$$\hat{\boldsymbol{d}} = \boldsymbol{D}\dot{\boldsymbol{q}} + \boldsymbol{d}_c \tag{23}$$

where the ith component of vector $\boldsymbol{d}_c$ is given by the model

$$d_{ci} = \begin{cases} D_{ci}\,\mathrm{sgn}(\dot{q}_i), & |\dot{q}_i| \geq \dot{q}_{si} \\ \dfrac{D_{ci}}{\dot{q}_{si}}\,\dot{q}_i, & |\dot{q}_i| < \dot{q}_{si} \end{cases} \tag{24}$$

where the D_{ci}'s are the estimated Coulomb friction coefficients and the $\dot{q}_{si}$'s are suitable velocity thresholds.

The same case study as above was developed. The results in Fig. 7 show that path tracking accuracy is improved, although at the expense of an undesirable chattering behavior on all components of contact force; this phenomenon, due to the Coulomb friction compensating term, could be mitigated by choosing a wider threshold, but tracking accuracy would then become worse again [32]. Therefore, in the remainder, compensation of static friction is no longer considered.

B. Impedance Control with Inner Position Loop

In order to reduce the effects of the disturbance term $\boldsymbol{\eta}$ on the system, a modified impedance control scheme can be designed by introducing an inner position loop [33]. The new control input in (17) is chosen as

$$\boldsymbol{a} = \ddot{\boldsymbol{p}}_r + \frac{k_v}{k_a}\,(\dot{\boldsymbol{p}}_r - \dot{\boldsymbol{p}}) + \frac{k_p}{k_a}\,(\boldsymbol{p}_r - \boldsymbol{p}) \tag{25}$$

where k_p, k_v, and k_a are the gains of the inner position control loop, the reference $\boldsymbol{p}_r$ of which is the solution to

$$m_d(\ddot{\boldsymbol{p}}_d - \ddot{\boldsymbol{p}}_r) + d_d(\dot{\boldsymbol{p}}_d - \dot{\boldsymbol{p}}_r) + k_d(\boldsymbol{p}_d - \boldsymbol{p}_r) = \boldsymbol{f} \tag{26}$$

characterizing the dynamics of the desired impedance. The dynamic behavior of system (1), (15), and (25) is then described by

$$k_a(\ddot{\boldsymbol{p}}_r - \ddot{\boldsymbol{p}}) + k_v(\dot{\boldsymbol{p}}_r - \dot{\boldsymbol{p}}) + k_p(\boldsymbol{p}_r - \boldsymbol{p}) = k_a\boldsymbol{\eta}. \tag{27}$$

Note that the gains of the inner position loop can be set independently of the impedance parameters and, thus, they are available to provide accurate position tracking of $\boldsymbol{p}_r$ and good disturbance rejection of $\boldsymbol{\eta}$. In fact, substituting the control law (15) and (25) in (1) and accounting for (26), (3), and (4)

gives at steady state the following end-effector position and contact force:

$$\boldsymbol{p}_\infty = \boldsymbol{n}\boldsymbol{n}^T\left(\frac{k_d}{k+k_d}\left(\boldsymbol{p}_d - \frac{k_a}{k_p}\,\boldsymbol{\eta}_\infty\right) + \frac{k}{k+k_d}\,\boldsymbol{p}_0\right)$$
$$+ (\boldsymbol{I} - \boldsymbol{n}\boldsymbol{n}^T)\left(\boldsymbol{p}_d - \frac{k_a}{k_p}\,\boldsymbol{\eta}_\infty\right) \tag{28}$$

$$\boldsymbol{f}_\infty = \frac{kk_d}{k+k_d}\,\boldsymbol{n}\boldsymbol{n}^T\left(\boldsymbol{p}_d - \frac{k_a}{k_p}\,\boldsymbol{\eta}_\infty - \boldsymbol{p}_0\right) \tag{29}$$

which reveals that k_p and k_a can be suitably chosen so as to reduce the effects of $\boldsymbol{\eta}_\infty$.

In order to show the performance of impedance control with inner position loop, a case study was developed on the experimental setup described in Section II.

The end effector was placed in the same initial position as for the previous case studies, and the same trajectory as for the case study described in Section IV-A was assigned. The impedance parameters in (26) were set to the same values as in the previous case study, while the inner position loop gains were set to $k_a = 1$ kg, $k_v = 90$ N·s/m, and $k_p = 2500$ N/m.

The results are presented in the upper part of Fig. 8 in terms of the desired (dashed) and the actual (solid) end-effector path, together with the time history of the contact force. As above, the approximate location (dotted) of the surface is illustrated on the plot of the end-effector path, while the instant of contact (dotted line) and the instant of the end of the motion trajectory (dashed line) are evidenced on the plot of the contact force.

It can be recognized that path tracking accuracy is noticeably improved with respect to that obtained with the previous scheme and now is very good; this confirms the effective rejection of the disturbance thanks to the inner position loop. In this respect, this scheme does not suffer from lack of compensation of static friction which, thus, becomes unnecessary.

On the other hand, the contact force along z is still limited during the transient and reaches an approximate value of 20 N at steady state, as wished with the choice of k_d above. As before, an appreciable value of contact friction force along y occurs that remains at steady state, while the good end-effector tracking accuracy essentially causes no contact friction along x by maintaining the motion in the yz plane.
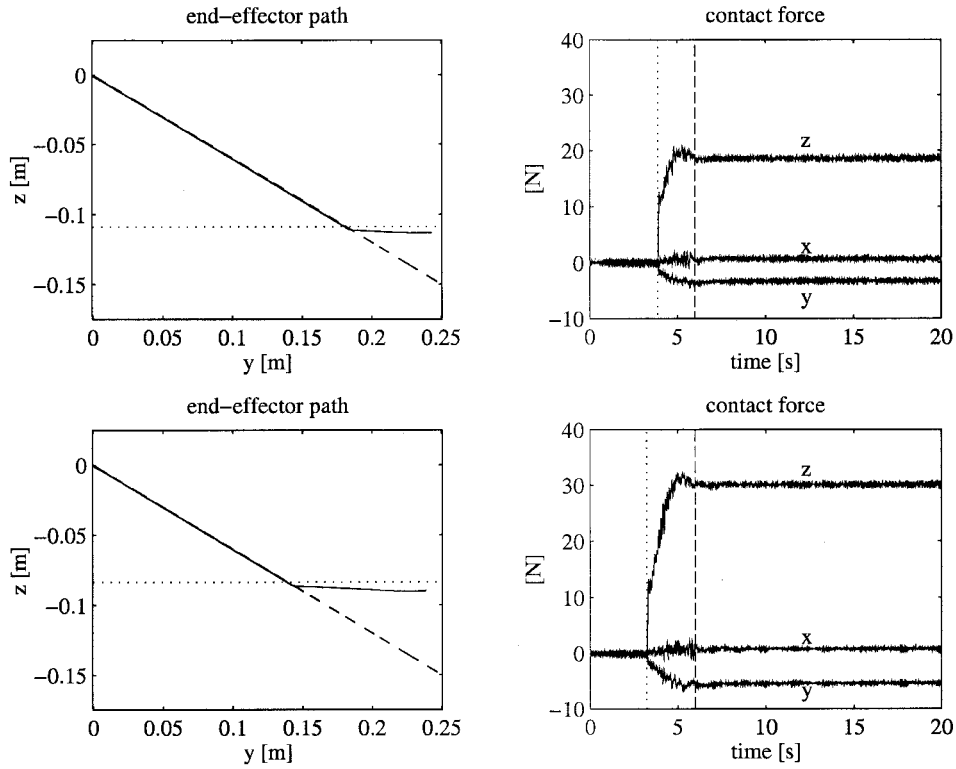
Fig. 8. Experimental results under impedance control with inner position loop.

To investigate robustness of the scheme with respect to changes in the environment location, the task was repeated with the same impedance parameters and inner position loop gains as before, but the cardboard box was raised by about 0.025 m. From the results presented in the lower part of Fig. 8, it can be recognized that the imposed motion would require the end effector to penetrate into the surface by a larger amount and, thus, the same value of k_d gives rise to a different (larger in this case) contact force at steady state. It is worth noticing that the larger value of contact force yields larger contact friction as well.

C. Force Control with Inner Velocity Loop

The above impedance schemes are aimed at controlling the contact force indirectly. If direct force control is desired, a force loop shall be designed acting upon the force error between the desired value f_d and the actual value f, as already done in Section IV-B. Differently from the control law (9) and (10) which requires an integral action on the force error—even in the absence of disturbances—a proportional action would now suffice to achieve force regulation, thanks to the dynamic model-based compensation.

In fact, in order to achieve a good dynamic behavior, the new control input should be of PD type on the force error. Force measures, however, are typically corrupted by noise, and then a derivative action on the contact force cannot be implemented in practice. As an alternative, in view of the model (3), a damping action can be provided by end-effector velocity feedback; this corresponds to using

an inner velocity loop—instead of the inner position loop in Section IV-B—while closing an outer force loop [5]. Hence, the new control input in (17) is chosen as

$$a = -\frac{k_v}{k_a}\,\dot{p} + \frac{k_p}{k_a}\,p_f \tag{30}$$

with

$$p_f = k_c(f_d - f) \tag{31}$$

where k_c is the gain of a proportional action on the force error.

Substituting the control law (15), (30), and (31) in (1) and accounting for (3) and (4) gives at steady state the contact force

$$f_\infty = f_d - \frac{k_a}{k_p k_c}\,nn^T\eta_\infty \tag{32}$$

which reveals that k_c, k_p, and k_a can be suitably chosen so as to reduce the effects of η_∞.

In order to show the performance of force control with inner velocity loop, a case study was developed on the experimental setup described in Section II.

The end effector was placed in the same initial position as for the previous case studies, but, of course, no trajectory could be assigned to the end-effector position. The desired force trajectory was the same as in the case study described in Section IV-B. The gains of the control action in (30) and (31) were set to $k_a = 1$ kg, $k_v = 60$ N·s/m, $k_p = 2500$ N/m, and $k_c = 0.00005$ N/(m·s).
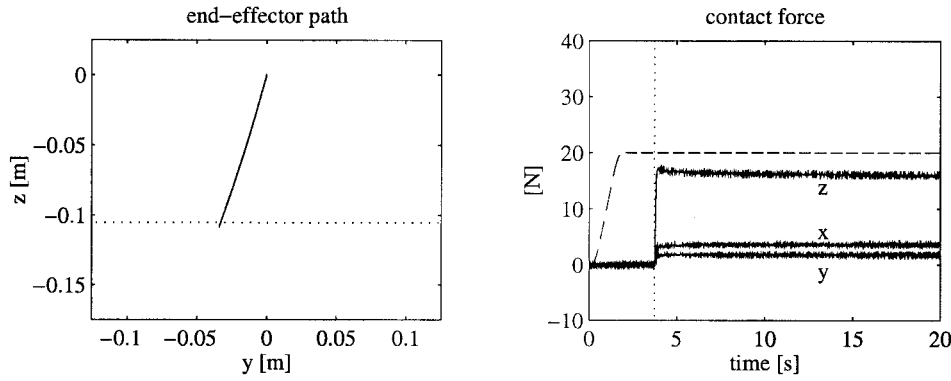
Fig. 9.   Experimental results under force control with inner velocity loop.

The results are presented in Fig. 9 in terms of the end-effector path, together with the time history of the desired (dashed) and the actual (solid) contact force. As above, the approximate location (dotted) of the surface is illustrated on the plot of the end-effector path, while the instant of contact (dotted line) is evidenced on the plot of the contact force.

Initially, the desired force trajectory causes a downward motion with a drift along both x and y (although the former is not visible in the figure); this brings the end effector to come in contact with the surface at $t = 3.7$ s. Notice that such drift is caused by the disturbance and is not counteracted because of the absence of a position loop. It can be recognized that the contact force along z at steady state does not reach its target value; this is mainly imputable to the disturbance term in (32). Also, an appreciable value of contact friction force along both x and y occurs that remains at steady state, which is due to the presence of the surface opposing to the above drift motion.

D. Force Control with Inner Position Loop

In order to eliminate the disturbance at steady state in (32), it is advisable to introduce an integral action on the force error. This would be possible by suitably modifying (31), but the dynamic behavior of the closed-loop system might become critical in the face of the chosen gains. A more effective solution is to add an inner loop on the end-effector position, as already done in (9). Hence, the new control input in (17) is chosen as

$$\boldsymbol{a} = -\frac{k_v}{k_a}\,\dot{\boldsymbol{p}} + \frac{k_p}{k_a}\,(\boldsymbol{p}_f - \boldsymbol{p}) \tag{33}$$

where

$$\boldsymbol{p}_f = k_c(\boldsymbol{f}_d - \boldsymbol{f}) + k_{ic}\int_0^t (\boldsymbol{f}_d - \boldsymbol{f})\,d\tau. \tag{34}$$

Substituting the control law (15), (33), and (34) in (1) and accounting for (3) and (4) gives at steady state the contact force

$$\boldsymbol{f}_\infty = \boldsymbol{f}_d. \tag{35}$$

In order to show the performance of force control with inner position loop, a case study was developed on the experimental setup described in Section II.

The end effector was placed in the same initial position as for the previous case studies. No trajectory was assigned to the end-effector position, and the desired force trajectory was the same as in the case study described in Section IV-B. The gains of the control action in (33) and (34) were set to $k_a = 1$ kg, $k_v = 90$ N·s/m, $k_p = 2500$ N/m, $k_c = 0.00005$ m/N, and $k_{ic} = 0.015$ m/(N·s).

The results are presented in Fig. 10 in terms of the end-effector path, together with the time history of the desired (dashed) and the actual (solid) contact force. As above, the approximate location (dotted) of the surface is illustrated on the plot of the end-effector path, while the instant of contact (dotted line) is evidenced on the plot of the contact force.

Initially, the desired force trajectory causes a downward vertical motion that brings the end effector to come in contact with the surface at $t = 4.5$ s. On the other hand, the response of the contact force is faster than that with pure force control in Section IV-B thanks to the use of an inverse dynamics strategy which allows obtaining a larger bandwidth of the force loop without affecting stability. Moreover, differently from the case study in Section V-C, since no motion drift occurs this time, the contact friction force along both x and y is practically null.

E. Parallel Force/Position Control

In order to combine the features of impedance control and force control, a parallel force/position control [7] can be designed which has capabilities of controlling contact force along the unconstrained task-space direction and end-effector position along the constrained task-space directions. The new control input in (17) is chosen as the sum of a position control action and a force control action, i.e.,

$$\boldsymbol{a} = \boldsymbol{a}_p + \boldsymbol{a}_f \tag{36}$$

where $\boldsymbol{a}_f$ shall prevail over $\boldsymbol{a}_p$, so as to effectively handle the interaction.

In the face of the robustifying action provided by the inner position loop for both the above impedance and force control schemes, the two control actions are selected as [34]

$$\boldsymbol{a}_P = \ddot{\boldsymbol{p}}_d + \frac{k_v}{k_a}\,(\dot{\boldsymbol{p}}_d - \dot{\boldsymbol{p}}) + \frac{k_p}{k_a}\,(\boldsymbol{p}_d - \boldsymbol{p}) \tag{37}$$

$$\boldsymbol{a}_f = \ddot{\boldsymbol{\xi}} + \frac{k_v}{k_a}\,\dot{\boldsymbol{\xi}} + \frac{k_p}{k_a}\,\boldsymbol{\xi} \tag{38}$$
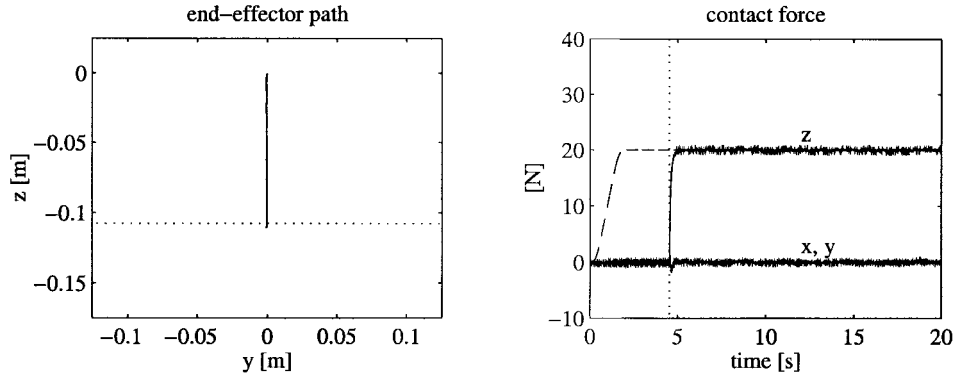
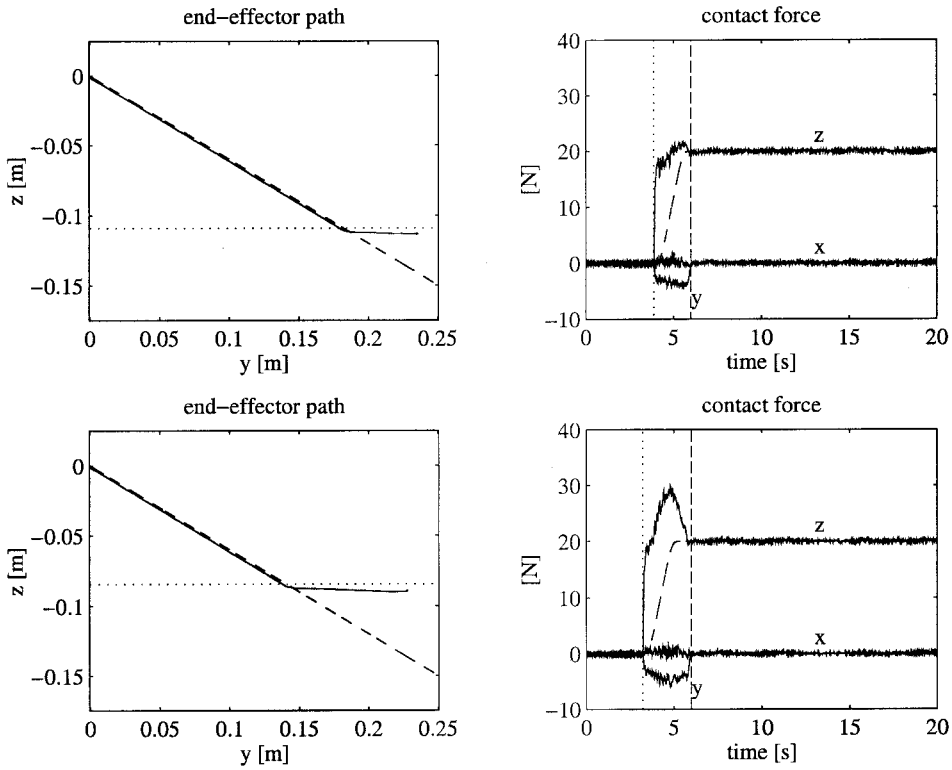Fig. 10. Experimental results under force control with inner position loop.

Fig. 11. Experimental results under parallel force/position control.

where $\boldsymbol{\xi}$ is the solution to

$$\ddot{\boldsymbol{\xi}} + \frac{k_b}{k_a}\,\dot{\boldsymbol{\xi}} = \frac{k_f}{k_a}\,(\boldsymbol{f}_d - \boldsymbol{f}). \qquad (39)$$

Notice that (38) and (39) yield an integral action on the force error—essential to guarantee the sought dominance of the force loop—and, moreover, they allow a desired dynamics of the force loop to be imposed through the gains k_f and k_b independently of the desired dynamics of the position loop set by the gains k_p, k_v, and k_a.

Substituting the control law (15) and (36)–(39) in (1) and accounting for (3) and (4) gives at steady state the following

end-effector position and contact force:

$$\boldsymbol{p}_\infty = \boldsymbol{n}\boldsymbol{n}^T\left(\frac{1}{k}\,\boldsymbol{f}_d + \boldsymbol{p}_0\right) + (\boldsymbol{I} - \boldsymbol{n}\boldsymbol{n}^T)\left(\boldsymbol{p}_d - \frac{k_a}{k_p}\,\boldsymbol{\eta}_\infty\right) \quad (40)$$

$$\boldsymbol{f}_\infty = \boldsymbol{f}_d \qquad (41)$$

which reveals that contact force is successfully regulated to the desired value, while the steady-state disturbance affects the end-effector components along the unconstrained task-space directions only.

In order to show the performance of parallel force/position control, a case study was developed on the experimental setup described in Section II.

The end effector was placed in the same initial position as for the previous case studies. The end-effector task was the

same as for the case study described in Section IV-A, while the same force trajectory as in Section IV-B started when contact was detected. The gains of the control action in (36)–(39) were set to $k_p = 2500$ N/m, $k_v = 90$ N·s/m, $k_a = 1$ kg, $k_f = 0.125$, and $k_b = 60$ N·s/m.

The results are presented in the upper part of Fig. 11 in terms of the desired (dashed) and the actual (solid) end-effector path, together with the time history of the desired (dashed) and the actual (solid) contact force. As above, the approximate location (dotted) of the surface is illustrated on the plot of the end-effector path, while the instant of contact (dotted line) and the instant of the end of the motion trajectory (dashed line) are evidenced on the plot of the contact force.

It can be recognized that path tracking accuracy is very good during unconstrained motion. On the other hand, the response of the contact force is faster than that with parallel regulator, for the same motivation regarding inverse dynamics as in the previous case study. As a consequence, the peak on the contact force along z is greatly reduced and successful regulation to the desired value is achieved. A smaller deformation of the surface occurs which also contributes to reducing the contact friction force along y by a factor of about two.

As for the case of impedance control with inner position loop in Section V-B, to investigate robustness of the scheme with respect to changes in the environment location, the task was repeated with the same control parameters as above, but the cardboard box was raised by about 0.025 m. From the results presented in the lower part of Fig. 11, it can be recognized that, despite the different location of the surface, the desired force set point is still achieved; however, larger values of contact force are obtained during the transient due to the larger impact velocity.

VI. CONCLUSION

A number of interaction control schemes were experimentally tested when the end effector of a robot manipulator comes in contact with a nearly flat surface, the location and stiffness of which are not exactly known.

The performance of the schemes using dynamic model-based compensation was shown to be generally superior to that of the schemes using static model-based compensation. A key point in the analysis has been disturbance rejection, in particular, in view of the inherent difficulties to obtain an accurate model of joint friction, as well as to include the effects of contact friction on the surface.

As an outcome of the present study, it has been recognized that it is advantageous to realize an inner loop on the end-effector position, while the force is effectively regulated to a desired value only with the use of an integral action on the force error.

Among all the various schemes, the parallel force/position control has given the most encouraging results in the light of its capabilities of controlling both the end-effector position along the unconstrained task-space directions and the contact force along the constrained task-space direction. The results obtained with impedance control are also good; however, the contact force depends on tuning of the impedance parameters in the face of the desired trajectory and environment stiffness and location.

The implementation was performed on an industrial robot with open control architecture; this allows a PC to be interfaced to the robot control unit with the possibility of using a wrist force sensor, as well as of achieving torque control. This is quite promising to foresee real applications of interaction control schemes on conventional industrial robots using model-based compensation and force measurement.

Only three-degree-of-freedom end-effector tasks were considered. Future research efforts will be devoted to extending the work to six-degree-of-freedom tasks with inclusion of end-effector orientation and contact moment.

REFERENCES

[1] D. E. Whitney, "Historical perspective and state of the art in robot force control," *Int. J. Robot. Res.*, vol. 6, no. 1, pp. 3–14, 1987.
[2] J. K. Salisbury, "Active stiffness control of a manipulator in Cartesian coordinates," in *Proc. 19th IEEE Conf. Decision and Control*, Albuquerque, NM, 1980, pp. 95–100.
[3] N. Hogan, "Impedance control: An approach to manipulation, Parts I–III," *ASME J. Dynam. Syst., Meas., Contr.*, vol. 107, pp. 1–24, 1985.
[4] D. E. Whitney, "Force feedback control of manipulator fine motions," *ASME J. Dynam. Syst., Meas., Contr.*, vol. 99, pp. 91–97, 1977.
[5] J. De Schutter and H. Van Brussel, "Compliant robot motion II. A control approach based on external control loops," *Int. J. Robot. Res.*, vol. 7, no. 4, pp. 18–33, 1988.
[6] R. Volpe and P. Khosla, "A theoretical and experimental investigation of explicit force control strategies for manipulators," *IEEE Trans. Automat. Contr.*, vol. 38, pp. 1634–1650, Nov. 1993.
[7] S. Chiaverini and L. Sciavicco, "The parallel approach to force/position control of robotic manipulators," *IEEE Trans. Robot. Automat.*, vol. 9, pp. 361–373, Aug. 1993.
[8] M. T. Mason, "Compliance and force control for computer controlled manipulators," *IEEE Trans. Syst., Man, Cybern.*, vol. SMC-6, pp. 418–432, June 1981.
[9] M. H. Raibert and J. J. Craig, "Hybrid position/force control of manipulators," *ASME J. Dynam. Syst., Meas., Contr.*, vol. 103, pp. 126–133, 1981.
[10] T. Yoshikawa, "Dynamic hybrid position/force control of robot manipulators—Description of hand constraints and calculation of joint driving force," *IEEE Trans. Robot. Automat.*, vol. RA-3, pp. 386–392, Oct. 1987.
[11] N. H. McClamroch and D. Wang, "Feedback stabilization and tracking of constrained robots," *IEEE Trans. Automat. Contr.*, vol. 33, pp. 419–426, May 1988.
[12] F. Dogliani, G. Magnani, and L. Sciavicco, "An open architecture industrial controller," *Newslett. IEEE Robot. Automat. Soc.*, vol. 7, no. 3, pp. 19–21, 1993.
[13] G. Hirzinger, J. Bals, B. Brunner, R. Koeppe, and M. Schedl, "Toward a new robot generation," in *Proc. 5th Int. Symp. Methods and Models in Automation and Robotics*, Międzyzdroje, Poland, 1998, pp. 747–762.
[14] M. Takegaki and S. Arimoto, "A new feedback method for dynamic control of manipulators," *ASME J. Dynam. Syst., Meas. Contr.*, vol. 103, pp. 119–125, 1981.
[15] J. T. Wen and S. Murphy, "Stability analysis of position and force control for robot arms," *IEEE Trans. Automat. Contr.*, vol. 36, pp. 365–371, Mar. 1991.
[16] L. S. Wilfinger, J. T. Wen, and S. H. Murphy, "Integral force control with robustness enhancement," *IEEE Contr. Syst. Mag.*, vol. 14, pp. 31–40, Feb. 1994.
[17] S. Chiaverini, B. Siciliano, and L. Villani, "Force position regulation of compliant robot manipulators," *IEEE Trans. Automat. Contr.*, vol. 39, pp. 647–652, Mar. 1994.
[18] L. Sciavicco and B. Siciliano, *Modeling and Control of Robot Manipulators*. New York: McGraw-Hill, 1996.
[19] O. Khatib, "A unified approach for motion and force control of robot manipulators: The operational space formulation," *IEEE Trans. Robot. Automat.*, vol. RA-3, pp. 43–53, Feb. 1987.
[20] F. Caccavale and P. Chiacchio, "Identification of dynamic parameters and feedforward control for a conventional industrial manipulator," *Contr. Eng. Practice*, vol. 2, pp. 1039–1050, 1994.
[21] G. Antonelli, F. Caccavale, and P. Chiacchio, "Experimental estimation of dynamic parameters for an industrial manipulator," in *Proc.*

2nd IMACS Symp. Mathematical Modeling, Vienna, Austria, 1997, pp. 667–672.

[22] C. Canudas de Wit, B. Siciliano, and G. Bastin, Eds., *Theory of Robot Control*. London, U.K.: Springer-Verlag, 1996.

[23] R. Kelly, R. Carelli, M. Amestegui, and R. Ortega, "Adaptive impedance control of robot manipulators," *IASTED Int. J. Robot. Automat.*, vol. 4, pp. 134–141, 1989.

[24] G. Niemeyer and J.-J. E. Slotine, "Performance in adaptive manipulator control," *Int. J. Robot. Res.*, vol. 10, pp. 149–161, 1991.

[25] R. Lozano and B. Brogliato, "Adaptive hybrid force-position control for redundant manipulators," *IEEE Trans. Automat. Contr.*, vol. 37, pp. 1501–1505, Oct. 1992.

[26] Z. Lu and A. A. Goldenberg, "Robust impedance control and force regulation: Theory and experiments," *Int. J. Robot. Res.*, vol. 14, pp. 225–254, 1995.

[27] B. Yao and M. Tomizuka, "Smooth robust adaptive sliding mode control of manipulators with guaranteed transient performance," *ASME J. Dynam. Syst., Meas., Contr.*, vol. 118, no. 4, pp. 764–775, 1996.

[28] B. Siciliano and L. Villani, "A passivity-based approach to force regulation and motion control of robot manipulators," *Automatica*, vol. 32, pp. 443–447, 1996.

[29] R. J. Anderson, "Dynamic damping control: Implementation issues and simulation results," in *Proc. IEEE Int. Conf. Robotics and Automation*, Cincinnati, OH, 1990, pp. 68–77.

[30] H. Kazerooni, B. Sheridan, and P. K. Houpt, "Robust compliant motion for manipulators—I: The fundamental concepts of compliant motion," *IEEE Trans. Robot. Automat.*, vol. RA-2, pp. 83–92, June 1986.

[31] H. Kazerooni, P. K. Houpt, and T. B. Sheridan, "Robust compliant motion for manipulators—II: Design method," *IEEE Trans. Robot. Automat.*, vol. RA-2, pp. 93–105, June 1986.

[32] F. Bruni, F. Caccavale, C. Natale, and L. Villani, "Experiments of impedance control on an industrial robot manipulator with joint friction," in *Proc. IEEE Int. Conf. Control Applications*, Dearborn, MI, 1996, pp. 205–210.

[33] W.-S. Lu and Q.-H. Meng, "Impedance control with adaptation for robotic manipulators," *IEEE Trans. Robot. Automat.*, vol. 7, pp. 408–415, June 1991.

[34] S. Chiaverini, B. Siciliano, and L. Villani, "Parallel force/position control schemes with experiments on an industrial robot manipulator," in *Proc. 13th IFAC World Congr.*, San Francisco, CA, 1996, vol. A, pp. 25–30.

Bruno Siciliano (M'91–SM'94) was born in Naples, Italy, in 1959. He received the Laurea degree and the Research Doctorate degree in electronic engineering from the University of Naples, Naples, Italy, in 1982 and 1987, respectively.

Since 1987, he has been with the Faculty of Engineering, University of Naples, where he is currently an Associate Professor of Robotics in the Department of Computer and Systems Engineering. From September 1985 to June 1986, he was a Visiting Scholar in the School of Mechanical Engineering, Georgia Institute of Technology. His research interests include manipulator inverse kinematics techniques, redundant manipulator control, modeling and control of flexible arms, force/motion control of manipulators, and cooperative robot manipulation. He has authored more than 150 published journal and conference papers. He is the co-author of *Modeling and Control of Robot Manipulators with Solutions Manual* (New York: McGraw-Hill, 1996) and *Theory of Robot Control* (London, U.K.: Springer-Verlag, 1996), and he is the co-editor of *Control Problems in Robotics and Automation* (London, U.K.: Springer-Verlag, 1998). He has delivered more than 70 invited seminars and presentations at international institutions. He was Associate Technical Editor of the *ASME Journal of Dynamic Systems, Measurement, and Control* from 1994 to 1999. He is also on the Editorial Advisory Boards of *Robotica* and the *JSME International Journal*. He has been on the program committees of several international robotics conferences.

Dr. Siciliano is a member of the American Society of Mechanical Engineers. He served as Associate Editor of the IEEE TRANSACTIONS ON ROBOTICS AND AUTOMATION from 1991 to 1994. Since 1996, he has been an Administrative Committee Member of the IEEE Robotics and Automation Society (re-elected in 1999), and Chair of the Technical Committee on Manufacturing and Automation Robotic Control of the IEEE Control Systems Society. In February 1999, he was appointed Vice-President for Publications of the IEEE Robotics and Automation Society. He was Program Chair of the IEEE International Workshop on Control Problems in Robotics and Automation: Future Directions (1997), Program Vice-Chair of the IEEE International Conference on Robotics and Automation (1998 and 1999), and he is General Co-Chair of the 1999 IEEE/ASME International Conference on Advanced Intelligent Mechatronics.

Stefano Chiaverini was born in Naples, Italy, in 1961. He received the Laurea degree and the Research Doctorate degree in electronic engineering from the University of Naples, Naples, Italy, in 1986 and 1990, respectively.

From 1990 to 1998, he was with the Department of Computer and Systems Engineering, University of Naples. He is currently an Associate Professor of Automatic Control in the Faculty of Engineering, University of Cassino, Cassino, Italy. From January to June 1989, he was a Visiting Scholar in the Robotics Laboratory of the German Aerospace Research Establishment (DLR). His research interests include manipulator inverse kinematics techniques, redundant manipulator control, force/motion control of manipulators, cooperative robot manipulation, and underwater robotics. He has authored more than 80 published journal and conference papers. He is the co-editor of *Complex Robotic Systems* (London, U.K.: Springer-Verlag, 1998).

Luigi Villani (S'94–M'96) was born in Avellino, Italy, in 1966. He received the Laurea degree and the Research Doctorate degree in electronic engineering from the University of Naples, Naples, Italy, in 1992 and 1996, respectively.

Since 1996, he has been with the Faculty of Engineering, University of Naples, where he is currently a Post-Doctoral Fellow of Robotics in the Department of Computer and Systems Engineering. From June to October 1995, he was a Visiting Scholar at the Laboratoire d'Automatique de Grenoble, Institut National Polytechnique de Grenoble. His research interests include force/motion control of manipulators and adaptive and nonlinear control of mechanical systems. He has authored more than 40 published journal and conference papers and is the co-author of *Solutions Manual to Accompany Modeling and Control of Robot Manipulators* (New York: McGraw-Hill, 1996).